

Line of Sight: On Linear Representations in VLLMs

Achyuta Rajaram^{1*} Sarah Schwettmann^{1,2} Jacob Andreas¹ Arthur Conmy

¹MIT CSAIL ²Transluce

*Primary Author, Correspondence to achyuta@mit.edu

Abstract

Language models can be equipped with multimodal capabilities by fine-tuning on embeddings of visual inputs. But how do such multimodal models represent images in their hidden activations? We explore representations of image concepts within LLaVA-Next, a popular open-source VLLM. We find a diverse set of ImageNet classes represented via linearly decodable features in the residual stream. We show that the features are causal by performing targeted edits on the model output. In order to increase the diversity of the studied linear features, we train multimodal Sparse Autoencoders (SAEs), creating a highly interpretable dictionary of text and image features. We find that although model representations across modalities are quite disjoint, they become increasingly shared in deeper layers. Project page: <https://github.com/multimodal-interpretability/multimodal-saes>

1. Introduction

Vision-Language Models (VLLMs) that map multimodal input to text output have shown immense promise as tools in many visual tasks, from image captioning to question answering [2, 27]. VLLMs are usually trained by fine-tuning a pre-trained LLM backbone on the outputs of a pre-trained image encoder end-to-end for captioning tasks. This training approach has achieved strong performance on standard benchmarks, using small amounts of multimodal data while leveraging internet-scale pre-training for image and text understanding [2, 27, 32].

However, LLM fine-tuning is known to be a fairly “shallow” process, primarily enhancing existing neural circuitry [22, 43]. Given this, we ask: are VLLM representations of visual concepts novel and distinct from existing LLM representations, or are they simply superficial extensions?

We focus our efforts on interpreting LLaVA-Next 7b, a model trained by fine-tuning a Vicuna 7b pre-trained LLM [42] alongside a CLIP [44] image encoder on end-to-end multimodal instruction following, connected by a two-layer MLP projection. We extend previous work on linear repre-

sentations in language-only models to study learned representations within LLaVA Next’s transformer decoder, using tools including linear probes [1], steering vectors [51] and Sparse Autoencoders (SAEs; Bricken et al. [6], Cunningham et al. [12], Ng [35]).

First, we study how abstract image concepts are represented within the decoder-only language model, through both probing and intervention-based methods. We find that probing accurately recovers coarse image contents from the residual stream, as represented by ImageNet class, and steering allows us to edit image representations with a predictable effect on model outputs. Using causal interventions, we find that image information is transferred into text tokens in the early-mid layers of the model. Then, we study broader linear representations of text and image concepts. Using SAEs for unsupervised feature discovery, we generate monosemantic, interpretable, linear features within the model at scale. We find that linear features corresponding to ImageNet class are well-represented by the SAE basis. We also find evidence of representations becoming increasingly multimodal across layers, possibly related to the “stages of inference” [14, 26] of the VLLM.

2. Related Work

2.1. Interpreting Language Models

In recent years, extensive work has been done to interpret the internals of language models, to further understand the principles underlying model behavior. LLMs can be dissected into interpretable components in the space of weights [37], subgraphs [11], and activations [18, 50]. Such interpretability techniques have found use for applications such as knowledge erasure [31], and behavior editing [52].

2.2. Interpreting Vision Models

The widespread application of neural networks for computer vision has inspired efforts to understand the mechanisms behind their performance. Previous work has extensively studied the impact of individual neurons [4, 21], as well as found linear, distributed representations using probing [1]. Furthermore, such linear representations have been used

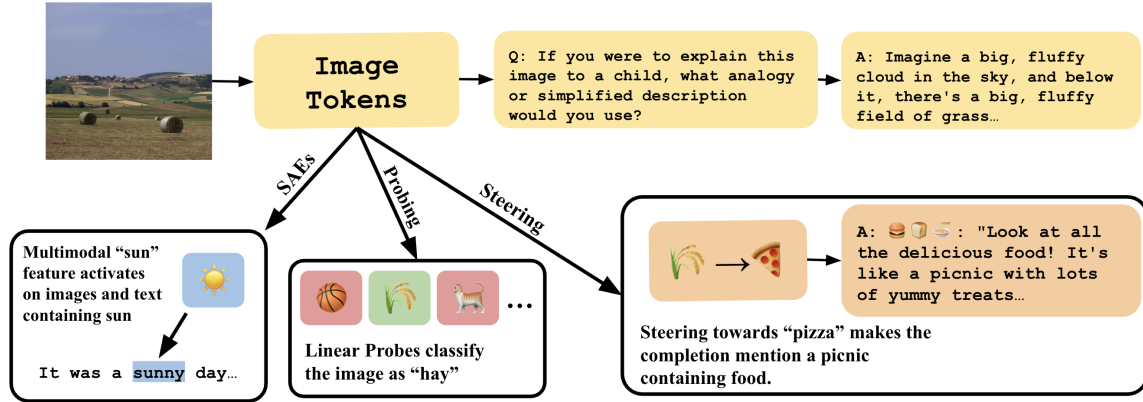


Figure 1. **Linear Representations of Image Information** A schematic diagram of linear probes, steering vectors, and Sparse Autoencoders as methods for analysing linear features derived from image tokens.

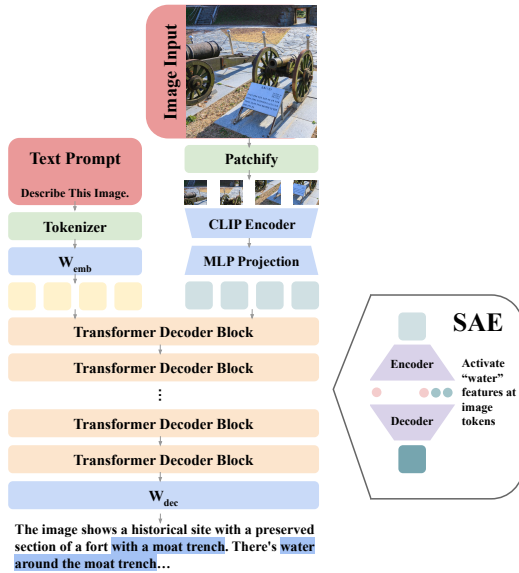


Figure 2. **Schematic of LLaVA-Next SAE Interventions:** text and image embeddings are processed separately, with the results projected into a shared latent space. If a water-related SAE feature is activated on all image tokens, the generated description of a cannon on dry land contains a hallucinated moat filled with water.

to perform intervention-level analysis on generative image models [53]. More recently, work has been done on finding interpretable subgraphs, as was done in language [46], as well as the discovery of latent structure within generative models [16].

2.3. Interpreting Vision-Language Models

Previous work on models like CLIP [44], and LIMBER [32] has focused on the model components which decode image information into text space [48]. More recent work

[23, 34] focuses on understanding VLLM representations through more sophisticated text-based methods, including the *logit lens* [36], as well as localizing the locations of specific objects in token space. They find success in applications including hallucination mitigation. In this work, we focus on intervention studies instead to localize the image-to-text computation pathway, as well as explore more general linear representations of images and text within the model.

3. Methods

3.1. Linear Probes

A hypothesis about how internal concepts are structured in decoder-only transformer language models is that they exist as one-dimensional linear subspaces within the residual stream (the output of transformer blocks) [41]. Such features have been used for decoding concepts within the residual stream [33], and controlling model behavior [51].

Despite this success, several pieces of simple information appear to be encoded nonlinearly (e.g. the days of the week in Engels et al. [15]). Thus, we ask: to what extent are image semantics encoded as linear features in LLaVA-Next? To do this, we train *linear probes*, linear classifiers over hidden activations, which have been used as tools for detecting the presence of encodings of concepts within models in previous work [1].

We use *linear probes* as classifiers for image information. Given a dataset of images $I_1, I_2, I_3, \dots \in D$, where each image belongs to exactly one of C classes, we compute *residual stream embeddings* $R_i \in \mathbb{R}^{h_{\text{dim}}}$ by taking the mean of the residual stream activations across all image token positions at a specified layer of the language model. Using these embeddings, we use Adam [24] to train a multiclass linear regression model, using a single linear layer to classify the residual stream states.

3.2. Steering Vectors

While linear probes are useful tools for localizing information within a model, they can often find features that are not causally relevant to the model [5]. If we wish to conclude that the model *uses* individual vector directions to represent concepts, we need to prove that the directions have effects on model outputs. Thus, we follow Giulianelli et al. [19], Turner et al. [51] and use *steering vectors*, a method for directly intervening on model behavior.

As in Turner et al. [51], we define *positive* and *negative* concepts (the class of the steering target, and the class of the source image, respectively), and sample images from each class. In keeping with our linear probing experiments, we compute *residual stream embeddings* for all the images. After taking the mean of the embeddings across the positive and negative classes (random pairs of classes), we subtract the embeddings to compute the resulting steering vectors, as is done in Panickssery et al. [40], a process called Contrastive Activation Addition (CAA). We then steer the model by adding in a constant vector at all image token positions at a specified layer.

In order to evaluate the resulting vectors, we attempt to steer the model to output captions relevant to the positive concept when provided an image of the negative (original) concept. A schematic of this approach is present in Figure 6a.

3.3. Training Sparse Autoencoders on VLLMs

Several works have studied methods for efficient sparse codes ([38, 49]); contemporary Sparse AutoEncoders (SAEs) are two-layer MLPs trained to reconstruct hidden layer activations of a larger model [35] in order to decompose its activations. SAEs have been used as tools for unsupervised disentanglement of computational structure in language models, from features [18, 50] to circuits [30]. In this work, we seek to extend this technique to vision-language models, to allow for the discovery of image-space and multimodal features. While Templeton et al. [50] find multimodal representations in Claude using text only SAEs (i.e., the golden gate bridge detector), we extend this technique to open VLLMs by training SAEs on joint text and image data, allowing us to isolate image representations.

Previous work trained SAEs on massive text datasets such as the Pile [17]. More recently, Kissane et al. [25] demonstrated that the distribution of learned SAE features is highly dataset-dependent. Thus to train multimodal SAEs that capture both text and image features, it is imperative to use a high-quality source of paired image-text data, as well as to balance the number of text and image tokens used. We use the training split of ShareGPT4V [10], a diverse image-caption dataset containing 1.2 million captioned images.

We train residual-stream SAEs in the text-only decoder of LLaVA-Next, borrowing the architecture and training process

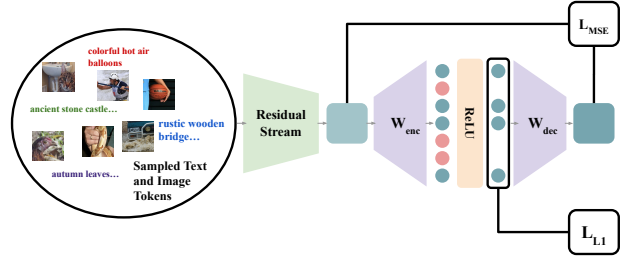


Figure 3. **Sparse Autoencoder Training:** From an image-text dataset D , we sample activations from random image and text tokens. We train a Sparse Autoencoder (SAE) to reconstruct the residual stream activations, using a sparse latent dictionary (L1 penalized).

from Templeton et al. [50], with no major changes. We use a ReLU activation function, and train to minimize reconstruction error (as measured by mean-squared error), as well as maximize sparsity (as approximated by the L1 across the hidden layer activations). We use $5e-5$ as the learning rate with an Adam Optimizer, decaying the learning rate to zero over the last 20 percent of training. We use an 8x expansion factor, yielding 32k SAE features in the learned dictionary, and an average L0 of 5. We use a density factor, $\lambda = 5$, as is the suggested default, and linearly increase it from $\lambda = 0$ over the first 5 percent of training steps. We train for 1.5 Billion tokens at a batch size of 4096, shuffling batches for a mix of image and text tokens. We follow Gao et al. [18] and train 5 SAEs on activations from the middle layers of the model, layers 8, 12, 16, 20, 24.

3.4. Evaluating Sparse Autoencoders

In order to test if the trained SAEs accurately approximate model behavior, we perform evaluation of the performance and interpretability of the suite of SAEs. As was done in prior work [45, 50], we report loss recovered, a measure of reconstruction fidelity which is computed by replacing activations with SAE reconstructions at a given layer and computing the fraction of CE loss recovered over a held out dataset. In our case, a held-out subset of ShareGPT-V is used, with the SAE reconstruction spliced on the text tokens, image tokens, and all tokens, at a given layer. We find that the loss recovered, compared to a baseline of zero ablation, is fairly competitive with work on language-only models [18, 50], (see Figure 4a).

We also evaluate the reconstruction fidelity by the use of VQA benchmarks, which provide a more comprehensive evaluation of vision-language model capabilities. Specifically, we use three popular benchmarks, MMMU, MMMU-PRO, and AOKVQA ([47, 54, 55]). We find that upon splicing in the SAE reconstructions for all image token features, the model only suffers a slight decrease in accuracy, illustrating that the SAEs capture visual features well (Figure

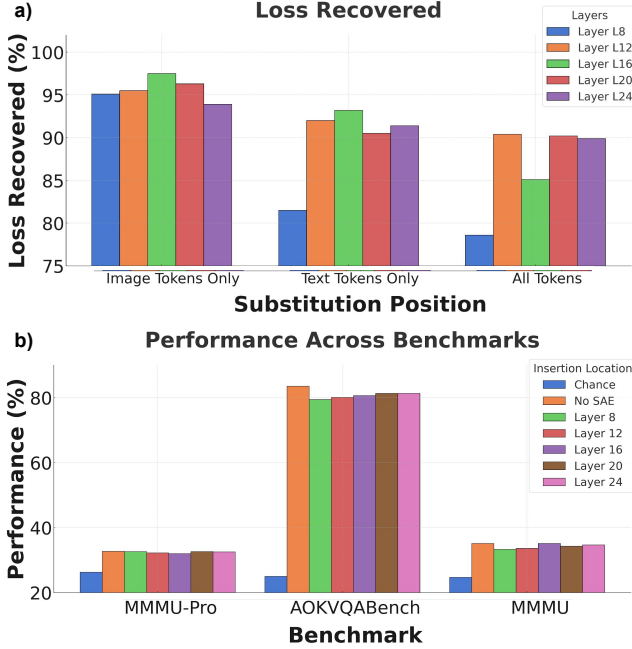


Figure 4. **SAE Evaluations.** We measure **a).** loss recovered and **b).** benchmark scores for the model with the SAE spliced in at various positions. We find that the SAEs reconstruct the information present in the image tokens well.

4 b.). However, upon splicing in the SAE at all token positions, instead of only image tokens, the accuracy drops to near chance, with the model failing to provide a coherent response. This is likely due to a distributional shift between the SAE training data (primarily vision-language captioning, with simple instructions) and the evaluation (more complex multiple-choice question answering).

3.5. Sparse Approximation of Steering Vectors

While our general SAE evaluations indicate that most model behaviors are contained within the SAE, we seek to ask questions about how the SAE represents specific features. Given a concept of interest (represented by a vector in $\mathbb{R}^{h_{\text{dim}}}$), we wish to know if the SAE contains it. One way to measure the SAE’s “knowledge” of a vector, is asking: can the SAE approximate the vector well with a small set of latents? To study this, we use the SAE *decoder matrix* as a sparse dictionary of vectors $\in \mathbb{R}^{h_{\text{dim}}}$. We optimize a sparse linear combination of the dictionary vectors, which reconstruct the concept of interest, as is done in Kissane et al. [25] and Rajamanoharan et al. [45]. The sparsity of the reconstruction (measured by L0), measures the extent to which the vector lies within the dictionary.

To construct sparse approximations of a vector, we follow [7, 28], and use the HardConcrete distribution [29] in order to directly perform gradient descent, optimizing the

coefficients of a linear combination on a joint objective of reconstruction accuracy (as measured by cosine similarity) and sparsity (as measured by the expected count of non-zero entries, $\mathbb{E}(\|\theta\|_0)$).

We can vary the sparsity of the resulting masks via an adjustable parameter λ , scaling the two terms in the loss. See Algorithm 1 for more details.

Algorithm 1 Sparse Dictionary Approximation via Learnable Binary Masking

- 1: **Input:** Target vector $v \in \mathbb{R}^{h_{\text{dim}}}$, dictionary W , sparsity weight λ , learning rate α , iterations T , temperature β , mask bounds $\gamma = -0.1, \zeta = 1.1$.
 - 2: Initialize dictionary coefficients x and mask logits θ (both matching W ’s feature dimension).
 - 3: **for** $t = 1$ to T **do**
 - 4: Sample noise $U \sim \text{Unif}(0, 1)$ (same shape as θ).
 - 5: Compute soft mask: $S = \sigma\left(\frac{1}{\beta}(\log \frac{U}{1-U} + \theta)\right)$.
 - 6: Apply hard bounds: $z = \min(1, \max(0, S(\zeta - \gamma) + \gamma))$.
 - 7: Reconstruct: $\hat{v} = W(x \odot z)$ where \odot denotes element-wise product.
 - 8: Compute cosine reconstruction loss: $L_{\text{cos}} = 1 - \frac{\hat{v} \cdot v}{\|\hat{v}\| \|v\|}$.
 - 9: Compute sparsity regularizer: $R(\theta) = \frac{1}{d} \sum_{i=1}^d \sigma\left(\theta_i - \beta \log \frac{-\gamma}{\zeta}\right)$.
 - 10: Total loss: $L = L_{\text{cos}} + \lambda R(\theta)$.
 - 11: Gradient updates: $x \leftarrow x - \alpha \nabla_x L$, $\theta \leftarrow \theta - \alpha \nabla_{\theta} L$.
 - 12: **end for**
 - 13: **Output:** Sparse representation as element-wise product of coefficients x and binary mask z .
-

4. How are Image Concepts Represented in the language model?

One natural set of visual concepts are those defined as classes in ImageNet [13]. We find that one-dimensional vectors in the residual stream represent the *ImageNet class* of a given image, and show that interventions on such vectors have predictable causal effects. Furthermore, we distinguish between the features generated by probing and steering-based techniques.

4.1. Does the residual stream contain the ImageNet class of a given image?

Yes. We train linear probes to perform ImageNet-1K classification, using the average image token representation at a fixed layer, and compare performance of the linear probes against modern self-supervised and supervised image classifiers, namely DINO [8], DINOv2 [39], CLIP [44], SIGLIP

[56], and ResNet-152 [20]. We find that linear classifiers trained throughout the model achieve strong performance, on par with classifiers trained directly on self-supervised image representations (Figure 5).

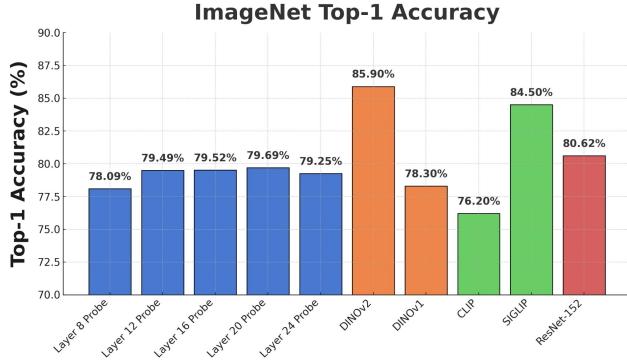


Figure 5. **ImageNet Accuracy.** We benchmark linear probes trained on mean embeddings across image tokens on ImageNet Classification. Performance is competitive with modern SSL techniques indicating linear representations of the class variable.

4.2. Can the residual stream be used to steer how models see images?

Yes. Previous work on steering vectors in language models [3, 51] uses a limited set of concepts, due to the difficulty of defining and collecting data for the positive and negative behaviors. As *positive* and *negative* concepts are easily defined in the image space, we scale our evaluation to 50 steering vectors, each defined by a randomly selected pair of ImageNet classes. We isolate steering vectors through CAA, and apply them at the layer of isolation, across several layers of the model. Some examples of the resulting model outputs are present in Appendix B.

To evaluate the efficacy of our steering vectors, we compute model completions conditioned on images of the negative class across a diverse set of questions (e.g. What are some key distinctive features or characteristics that make this thing unique?), while adding varied amounts of the steering vectors into the image tokens. As was done in Chalnev et al. [9], we use gpt4o-mini to rate the model completions on *coherence* and *steering amount*; an optimal steering vector would steer the model outputs towards the target class while maintaining a syntactically sound output (e.g. a flawless description of an image of the target would achieve maximum score on both metrics, while an empty string would achieve minimum coherence score, but neutral steering score.) We plot a Pareto Frontier of the two scores to compare sets of vectors.

In order to verify that our LLM Judge accurately scores model rollouts, we perform a human study of the coherence and steering scores, and measure agreement. For the

coherence score, we provide pairwise model rollouts to human graders, and ask the human graders to select the more grammatically correct rollout. Plotting human preferences against LLM Judge labels, we find strong correlation (Figure Fig. 6 d). For the steering score, we provide users with a model completion as well as four potential class labels, and ask them to select the most relevant class. We again find that the human answer selections correlate strongly with the LLM judge (Figure Fig. 6 e). More details on these human evaluations are present in Appendix A.

We perform steering across several layers, finding that targeted interventions can steer model output in a predictable fashion (Figure 6 b). As a side note, it appears that the steered outputs are not random; they are highly dependent on semantic facts about the original, uncorrupted image (Figure 1). For example, if one steers an image of hay bales on a farm towards the class “pizza”, the model describes a picnic scene, preserving that the image was taken outdoors.

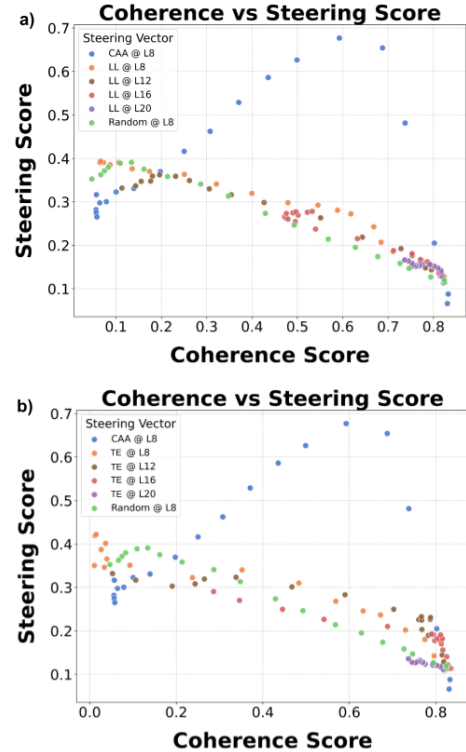


Figure 7. **Text-Based Steering Vectors** We measure coherence vs. steering score for steering vectors across several steering strengths. We find that both **a).** using the unembedding matrix (Logit Lens, abbreviated LL). and **b).** using the hidden layer activations as Text Embeddings (TE) are *ineffective* steering methods.

4.3. Where in the model is steering most effective?

Early to Middle Layers. From Figure 6 b., we see that the impact of steering vectors decreases between layers, or that

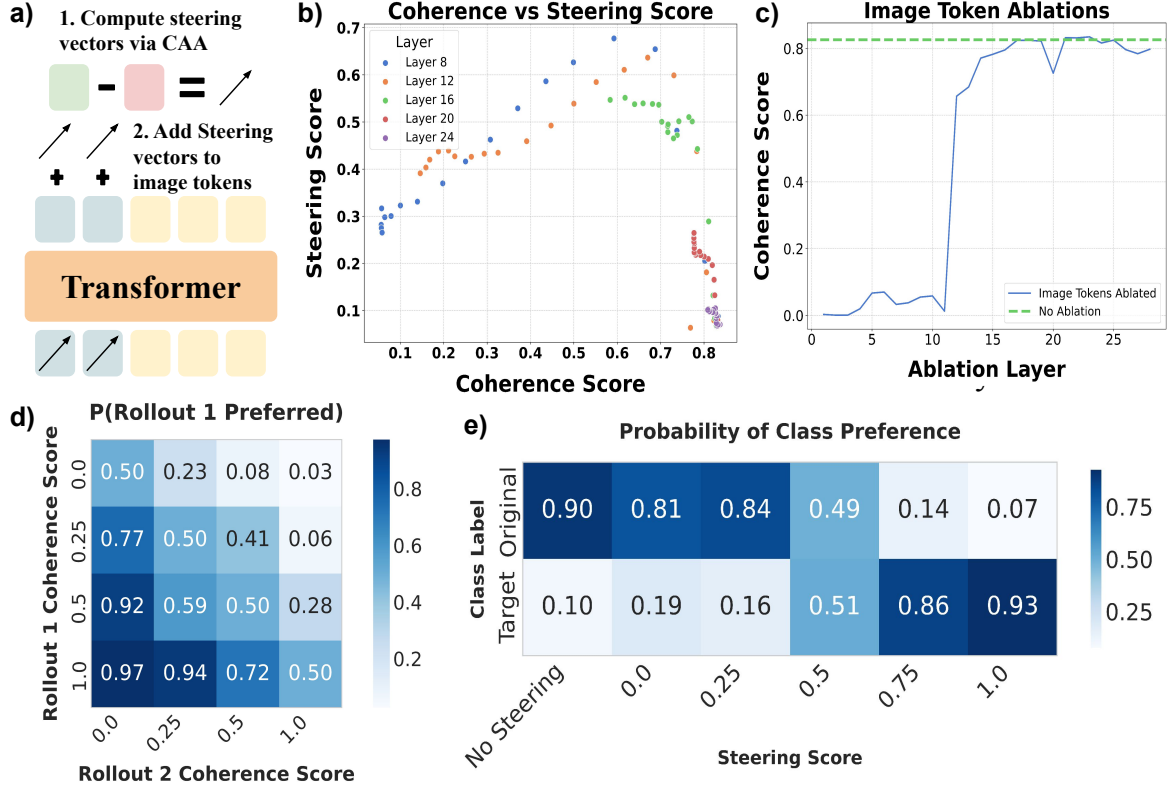


Figure 6. **Steering Vector Interventions** **a)**. Schematic Diagram of Steering Vectors. We compute them using activations from images of two classes, and add the resulting vectors in at image tokens. **b)**. We compute coherence and steering scores as measures of steering vector efficacy. We find that steering at earlier layers is more effective. **c)**. We zero-ablate all image tokens at each layer, to localize image information within the model forward pass. **d)**. We find that our LLM judge’s evaluations of sentence coherence align closely with human raters. **e)**. We find that our LLM judge’s evaluations of steering magnitude align closely with human raters.

interventions of the same magnitude in deeper layers have a less causal effect (as measured by our evaluations). We hypothesize that this effect is due to the model *not utilizing* the image tokens at late layers of the forward pass. We verify this by performing a targeted ablation: given a layer, we zero out the residual stream at all image tokens. We then measure the impact of the ablation by computing the *coherence score* of the model description (Figure 6 c). While ablating early layer image tokens is catastrophic for model performance, ablation effectiveness steeply declines halfway through the model. Ablations after layer 12 have a negligible effect on the coherence of model rollouts, indicating a well-defined location of “information transfer”.

4.4. Can Text-derived Features Steer Image Representations?

Not really. As LLaVA-Next is a vision-language model, one might wonder; does the model represent text and image features separately, or does the model use a shared code? Previous work has found some evidence for shared latents,

with the image features being increasingly represented in the text basis throughout the model layers [34], [23]. However, as we have seen in the case of linear probes, the existence of directions in a model’s residual stream does not necessarily imply that the model uses such directions for downstream tasks.

Thus, we perform a principled evaluation of text-based features for image token manipulation, attempting to steer model outputs with textual features. We perform two interventions, inspired by Jiang et al. [23] Logit Lens (LL), and Text Embeddings (TE).

LL computes steering vectors for ImageNet classes A,B by finding the unembedding vectors for the corresponding text tokens, as is done in nostalgebraist [36], subtracting them from each other, and normalizing. For TE, we instead pass the text tokens into the language model of the VLLM, extracting the residual stream at the layer of interest. We then use the resulting steering vectors to perform model interventions. We find that both of these text-derived vectors perform no better than random vectors, and are drastically

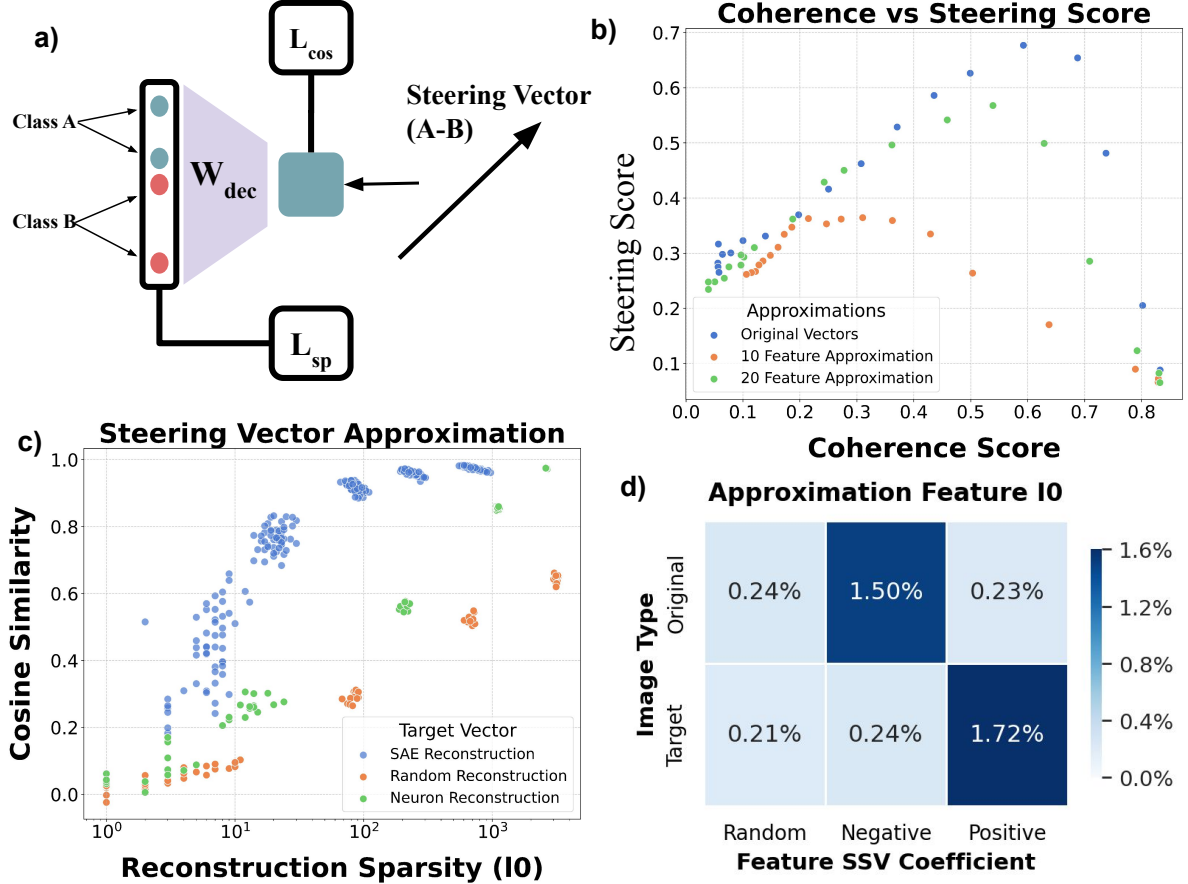


Figure 8. **SAE Steering Vector Approximation** **a)** A schematic diagram of the approximation process. We optimize SAE hidden latents, using the decoder matrix as a dictionary, for sparsity (L_{sp}) and reconstruction accuracy (L_{cos}). **b)** To measure approximation quality, we compute coherence and steering score. We achieve most of the effect of the dense steering vector with only 20 SAE features. **c)** We find that SAE features can approximate steering vectors well, with neurons forming a worse dictionary. **d)** We find that the coefficients of SAE features selected by the sparse approximation process represent semantic structure in the image.

outperformed by image space CAA features (Figure 13). This is unsurprising, as textual features are more present later in the model’s forward pass, but the model does not use late-layer image features for captioning (Figure 6 c).

5. What Features do SAEs recover?

In the previous section, we explored how LLaVa-Next represents a specific type of coarse image information: the ImageNet Class. However, we are interested in answering questions about more general concepts, both within images and text. To this end, we train SAEs, finding that they uncover a diverse family of multimodal features within the model’s residual stream activations. We find that even ImageNet Class is well-represented by our SAEs, pointing towards SAEs as a general tool for understanding visual representations within VLLMs.

5.1. Monosemantic, Multimodal Features

Previous work on SAEs in LLMs have found their recovered features to be highly interpretable and monosemantic, leading to their use as a tool for disentangling residual stream activations [50]. To this end, we benchmark the interpretability of our multimodal SAEs across image and text activations, using manual graders as is done in Rajamanoharan et al. [45]. We present a group of expert human raters with the activating examples of a randomly selected feature. The rater then decides if the feature has monosemantic text and image activations. If the human labeler finds that the descriptions match, a feature is deemed “multimodal”. We do the same process for all neurons. We find that SAEs are slightly more interpretable than neurons (Fig. 9 a), and that the proportion of multimodal features (and neurons) increases throughout the model (Fig. 9 b). Furthermore, we find that the neurons contain far more text-only features than the SAEs. More details on this evaluation are present in section C.

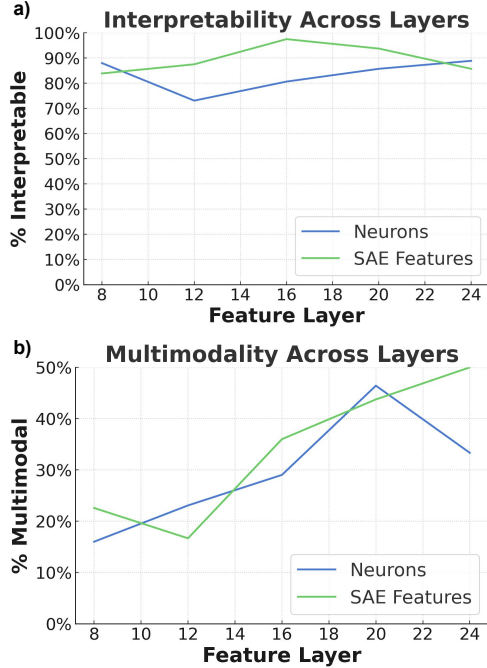


Figure 9. **Manual Interpretability Experiments a).** We find that SAE features are slightly more interpretable than neurons, but both are highly interpretable throughout the model. **b).** We find that our human raters are more likely to label both neurons and SAE features from later layers as “multimodal.”

5.2. ImageNet Class Features

We seek to measure how well the internal variable of ImageNet class is represented by the SAE. To approximate the internal representation of ImageNet class, we use the steering vectors outlined in Section 3.2, as we have shown that they form faithful approximations. We then perform the SDA algorithm as outlined in Algorithm 1, measuring the resulting sparsity. We find that the steering vectors are much “easier” to approximate than random vectors, requiring less than 100 SAE features to approximate well (Figure 8 c). Furthermore, we evaluate the resulting reconstructions on steering, as was done in section 2, and find that approximations with as few as 20 features perform comparably against the original steering vectors (Figure 8 b).

Finally, it is natural to ask: are the resulting sparse approximations composed of interpretable features? To answer this, we first group the features “selected” by the reconstruction (those with nonzero coefficient) into those positive and negative coefficients. When we consider their activation patterns across images, we find that these positive and negative features correspond directly to the positive and negative classes of the approximated steering vector, with predictable activations on images of the corresponding class (Figure 8 d).

6. Discussion

Through probing, steering, and SAE training, we find that diverse image-related variables exhibit linear structure; we use this to achieve fine-grained control of VLLM behavior. We also find evidence for multimodal representations organized in an “information hierarchy” across layers. Unlike in language models, we find that neurons form a highly interpretable basis over image information, comparing favorably to SAE features. We also find that linear representations have limitations—they provide an unnatural basis for image-space adversarial attacks (Appendix D). Future work should investigate the mechanisms underlying image-to-multimodal representation conversion and evaluate these findings across diverse VLLM architectures, particularly cross-attention-based models.

7. Acknowledgements

We are grateful for the support of the MIT-IBM Watson AI Lab, and ARL grant W911NF-18-2-0218. We thank David Bau, Caden Juang, and Yolanda Xie for their useful input and insightful discussions.

References

- [1] Guillaume Alain and Yoshua Bengio. Understanding intermediate layers using linear classifier probes, 2018.
- [2] Jean-Baptiste Alayrac, Jeff Donahue, Pauline Luc, Antoine Miech, Iain Barr, Yana Hasson, Karel Lenc, Arthur Mensch, Katie Millican, Malcolm Reynolds, Roman Ring, Eliza Rutherford, Serkan Cabi, Tengda Han, Zhitao Gong, Sina Samangooei, Marianne Monteiro, Jacob Menick, Sebastian Borgeaud, Andrew Brock, Aida Nematzadeh, Sahand Sharifzadeh, Mikolaj Binkowski, Ricardo Barreira, Oriol Vinyals, Andrew Zisserman, and Karen Simonyan. Flamingo: a visual language model for few-shot learning, 2022.
- [3] Andy Arditi, Oscar Obeso, Aaqib Syed, Daniel Paleka, Nina Panickssery, Wes Gurnee, and Neel Nanda. Refusal in language models is mediated by a single direction, 2024.
- [4] David Bau, Jun-Yan Zhu, Hendrik Strobelt, Agata Lapedriza, Bolei Zhou, and Antonio Torralba. Understanding the role of individual units in a deep neural network. *Proceedings of the National Academy of Sciences*, 117(48):30071–30078, 2020.
- [5] Yonatan Belinkov. Probing classifiers: Promises, shortcomings, and advances, 2021.
- [6] Trenton Bricken, Adly Templeton, Joshua Batson, Brian Chen, Adam Jermy, Tom Conerly, Nick Turner, Cem Anil, Carson Denison, Amanda Askell, Robert Lasenby, Yifan Wu, Shauna Kravec, Nicholas Schiefer, Tim Maxwell, Nicholas Joseph, Zac Hatfield-Dodds, Alex Tamkin, Karina Nguyen, Brayden McLean, Josiah E Burke, Tristan Hume, Shan Carter, Tom Henighan, and Christopher Olah. Towards monosemanticity: Decomposing language models with dictionary learning. *Transformer Circuits Thread*, 2023. <https://transformer-circuits.pub/2023/monosemantic-features/index.html>.
- [7] Steven Cao, Victor Sanh, and Alexander M. Rush. Low-complexity probing via finding subnetworks, 2021.
- [8] Mathilde Caron, Hugo Touvron, Ishan Misra, Hervé Jégou, Julien Mairal, Piotr Bojanowski, and Armand Joulin. Emerging properties in self-supervised vision transformers, 2021.
- [9] Sviatoslav Chalnev, Matthew Siu, and Arthur Conmy. Improving steering vectors by targeting sparse autoencoder features, 2024.
- [10] Lin Chen, Jinsong Li, Xiaoyi Dong, Pan Zhang, Conghui He, Jiaqi Wang, Feng Zhao, and Dahua Lin. Sharegpt4v: Improving large multi-modal models with better captions, 2023.
- [11] Arthur Conmy, Augustine N. Mavor-Parker, Aengus Lynch, Stefan Heimersheim, and Adrià Garriga-Alonso. Towards automated circuit discovery for mechanistic interpretability, 2023.
- [12] Hoagy Cunningham, Aidan Ewart, Logan Riggs, Robert Huben, and Lee Sharkey. Sparse autoencoders find highly interpretable features in language models. *arXiv preprint arXiv:2401.01345*, 2024.
- [13] Jia Deng, Wei Dong, Richard Socher, Li-Jia Li, Kai Li, and Li Fei-Fei. Imagenet: A large-scale hierarchical image database. In *2009 IEEE Conference on Computer Vision and Pattern Recognition*, pages 248–255, 2009.
- [14] Nelson Elhage, Tristan Hume, Catherine Olsson, Neel Nanda, Tom Henighan, Scott Johnston, Sheer ElShowk, Nicholas Joseph, Nova DasSarma, Ben Mann, Danny Hernandez, Amanda Askell, Kamal Ndousse, Andy Jones, Dawn Drain, Anna Chen, Yuntao Bai, Deep Ganguli, Liane Lovitt, Zac Hatfield-Dodds, Jackson Kernion, Tom Conerly, Shauna Kravec, Stanislav Fort, Saurav Kadavath, Josh Jacobson, Eli Tran-Johnson, Jared Kaplan, Jack Clark, Tom Brown, Sam McCandlish, Dario Amodei, and Christopher Olah. Softmax linear units. *Transformer Circuits Thread*, 2022. <https://transformer-circuits.pub/2022/solu/index.html>.
- [15] Joshua Engels, Eric J. Michaud, Isaac Liao, Wes Gurnee, and Max Tegmark. Not all language model features are linear, 2024.
- [16] Rohit Gandikota, Joanna Materzynska, Tingrui Zhou, Antonio Torralba, and David Bau. Concept sliders: Lora adaptors for precise control in diffusion models, 2023.
- [17] Leo Gao, Stella Biderman, Sid Black, Laurence Golding, Travis Hoppe, Charles Foster, Jason Phang, Horace He, Anish Thite, Noa Nabeshima, Shawn Presser, and Connor Leahy. The pile: An 800gb dataset of diverse text for language modeling, 2020.
- [18] Leo Gao, Tom Dupré la Tour, Henk Tillman, Gabriel Goh, Rajan Troll, Alec Radford, Ilya Sutskever, Jan Leike, and Jeffrey Wu. Scaling and evaluating sparse autoencoders, 2024.
- [19] Mario Giulianelli, Jacqueline Harding, Florian Mohnert, Dieuwke Hupkes, and Willem Zuidema. Under the hood: Using diagnostic classifiers to investigate and improve how language models track agreement information, 2021.
- [20] Kaiming He, Xiangyu Zhang, Shaoqing Ren, and Jian Sun. Deep residual learning for image recognition, 2015.
- [21] Evan Hernandez, Sarah Schwettmann, David Bau, Teona Bagashvili, Antonio Torralba, and Jacob Andreas. Natural language descriptions of deep visual features. In *International Conference on Learning Representations*, 2022.
- [22] Samyak Jain, Robert Kirk, Ekdeep Singh Lubana, Robert P. Dick, Hidenori Tanaka, Edward Grefenstette, Tim Rocktäschel, and David Scott Krueger. Mechanistically analyzing the effects of fine-tuning on procedurally defined tasks, 2024.
- [23] Nick Jiang, Anish Kachinthaya, Suzie Petryk, and Yossi Gandelsman. Interpreting and editing vision-language representations to mitigate hallucinations, 2024.
- [24] Diederik P. Kingma and Jimmy Ba. Adam: A method for stochastic optimization, 2017.
- [25] Connor Kissane, robertzk, Neel Nanda, and Arthur Conmy. Saes are highly dataset dependent: a case study on the refusal direction. 2024.
- [26] Vedang Lad, Wes Gurnee, and Max Tegmark. The remarkable robustness of llms: Stages of inference?, 2024.
- [27] Haotian Liu, Chunyuan Li, Yuheng Li, Bo Li, Yuanhan Zhang, Sheng Shen, and Yong Jae Lee. Llava-next: Improved reasoning, ocr, and world knowledge, 2024.
- [28] Christos Louizos, Max Welling, and Diederik P. Kingma. Learning sparse neural networks through l_0 regularization, 2018.

- [29] Chris J. Maddison, Andriy Mnih, and Yee Whye Teh. The concrete distribution: A continuous relaxation of discrete random variables, 2017.
- [30] Samuel Marks, Can Rager, Eric J. Michaud, Yonatan Belinkov, David Bau, and Aaron Mueller. Sparse feature circuits: Discovering and editing interpretable causal graphs in language models, 2024.
- [31] Kevin Meng, Arnab Sen Sharma, Alex Andonian, Yonatan Belinkov, and David Bau. Mass-editing memory in a transformer, 2023.
- [32] Jack Merullo, Louis Castricato, Carsten Eickhoff, and Ellie Pavlick. Linearly mapping from image to text space, 2023.
- [33] Neel Nanda, Andrew Lee, and Martin Wattenberg. Emergent linear representations in world models of self-supervised sequence models, 2023.
- [34] Clement Neo, Luke Ong, Philip Torr, Mor Geva, David Krueger, and Fazl Barez. Towards interpreting visual information processing in vision-language models, 2024.
- [35] Andrew Ng. Sparse autoencoder. *CS294A Lecture Notes*, 2011. Unpublished lecture notes.
- [36] nostalgebraist. interpreting GPT: the logit lens — LessWrong — lesswrong.com. <https://www.lesswrong.com/posts/AcKRB8wDpdan6v6ru/interpreting-gpt-the-logit-lens>. [Accessed 26-01-2025].
- [37] Kai Nylund, Suchin Gururangan, and Noah A. Smith. Time is encoded in the weights of finetuned language models, 2023.
- [38] Bruno A. Olshausen and David J. Field. Sparse coding with an overcomplete basis set: A strategy employed by v1? *Vision Research*, 37(23):3311–3325, 1997.
- [39] Maxime Oquab, Timothée Darcet, Théo Moutakanni, Huy Vo, Marc Szafraniec, Vasil Khalidov, Pierre Fernandez, Daniel Haziza, Francisco Massa, Alaaeldin El-Nouby, Mahmoud Assran, Nicolas Ballas, Wojciech Galuba, Russell Howes, Po-Yao Huang, Shang-Wen Li, Ishan Misra, Michael Rabbat, Vasu Sharma, Gabriel Synnaeve, Hu Xu, Hervé Jegou, Julien Mairal, Patrick Labatut, Armand Joulin, and Piotr Bojanowski. Dinov2: Learning robust visual features without supervision, 2024.
- [40] Nina Panickssery, Nick Gabrieli, Julian Schulz, Meg Tong, Evan Hubinger, and Alexander Matt Turner. Steering llama 2 via contrastive activation addition, 2024.
- [41] Kiho Park, Yo Joong Choe, and Victor Veitch. The linear representation hypothesis and the geometry of large language models, 2024.
- [42] Baolin Peng, Chunyuan Li, Pengcheng He, Michel Galley, and Jianfeng Gao. Instruction tuning with gpt-4, 2023.
- [43] Nikhil Prakash, Tamar Rott Shaham, Tal Haklay, Yonatan Belinkov, and David Bau. Fine-tuning enhances existing mechanisms: A case study on entity tracking, 2024.
- [44] Alec Radford, Jong Wook Kim, Chris Hallacy, Aditya Ramesh, Gabriel Goh, Sandhini Agarwal, Girish Sastry, Amanda Askell, Pamela Mishkin, Jack Clark, Gretchen Krueger, and Ilya Sutskever. Learning transferable visual models from natural language supervision, 2021.
- [45] Senthoooran Rajamanoharan, Arthur Conmy, Lewis Smith, Tom Lieberum, Vikrant Varma, János Kramár, Rohin Shah, and Neel Nanda. Improving dictionary learning with gated sparse autoencoders, 2024.
- [46] Achyuta Rajaram, Neil Chowdhury, Antonio Torralba, Jacob Andreas, and Sarah Schwettmann. Automatic discovery of visual circuits, 2024.
- [47] Dustin Schwenk, Apoorv Khandelwal, Christopher Clark, Kenneth Marino, and Roozbeh Mottaghi. A-okvqa: A benchmark for visual question answering using world knowledge, 2022.
- [48] Sarah Schwettmann, Neil Chowdhury, Samuel Klein, David Bau, and Antonio Torralba. Multimodal neurons in pretrained text-only transformers, 2023.
- [49] Bernhard Schölkopf, John Platt, and Thomas Hofmann. *Efficient sparse coding algorithms*, pages 801–808. 2007.
- [50] Adly Templeton, Tom Conerly, Jonathan Marcus, Jack Lindsey, Trenton Bricken, Brian Chen, Adam Pearce, Craig Citro, Emmanuel Ameisen, Andy Jones, Hoagy Cunningham, Nicholas L Turner, Callum McDougall, Monte MacDiarmid, C. Daniel Freeman, Theodore R. Sumers, Edward Rees, Joshua Batson, Adam Jermyn, Shan Carter, Chris Olah, and Tom Henighan. Scaling monosemanticity: Extracting interpretable features from claude 3 sonnet. *Transformer Circuits Thread*, 2024.
- [51] Alexander Matt Turner, Lisa Thiergart, Gavin Leech, David Udell, Juan J. Vazquez, Ulisse Mini, and Monte MacDiarmid. Steering language models with activation engineering, 2024.
- [52] Zhengxuan Wu, Aryaman Arora, Zheng Wang, Atticus Geiger, Dan Jurafsky, Christopher D. Manning, and Christopher Potts. Refit: Representation finetuning for language models, 2024.
- [53] Jianjin Xu and Changxi Zheng. Linear semantics in generative adversarial networks, 2021.
- [54] Xiang Yue, Yuansheng Ni, Kai Zhang, Tianyu Zheng, Ruoqi Liu, Ge Zhang, Samuel Stevens, Dongfu Jiang, Weiming Ren, Yuxuan Sun, Cong Wei, Botao Yu, Ruibin Yuan, Renliang Sun, Ming Yin, Boyuan Zheng, Zhenzhu Yang, Yibo Liu, Wenhao Huang, Huan Sun, Yu Su, and Wenhui Chen. Mmmu: A massive multi-discipline multimodal understanding and reasoning benchmark for expert agi, 2024.
- [55] Xiang Yue, Tianyu Zheng, Yuansheng Ni, Yubo Wang, Kai Zhang, Shengbang Tong, Yuxuan Sun, Botao Yu, Ge Zhang, Huan Sun, Yu Su, Wenhui Chen, and Graham Neubig. Mmmu-pro: A more robust multi-discipline multimodal understanding benchmark, 2024.
- [56] Xiaohua Zhai, Basil Mustafa, Alexander Kolesnikov, and Lucas Beyer. Sigmoid loss for language image pre-training, 2023.

A. Steering Vector Evaluation Details

We evaluate steering vectors on steering model answers to general VQA questions. To do this, we select 200 random pairs of ImageNet Classes, and steer from the first element of each pair to the other. We ask the model to answer the following questions with a 200-token completion, for each input image:

INST what is shown in this image? [/INST]

INST is this image related in any way to the concept {cls[cls_index]}? [/INST]

INST is this image related in any way to the concept {cls2[cls_index]}? [/INST]

INST Describe the primary purpose or function of the entity shown in this image? [/INST]

INST If you were to explain this image to a child, what analogy or simplified description would you use? [/INST]

INST In what environment or setting would you most likely encounter this? [/INST]

INST what are some key distinctive features or characteristics that make this thing unique? [/INST]

INST How large is the main subject of this image typically? [/INST]

INST Is this image more related to the concept {cls1[cls_index]} or the concept {cls2[cls_index]}? [/INST]

In order to evaluate the efficacy of our steering vectors, we use a gpt4o-mini LLM judge with the following prompts, for measuring steering amount and textual coherence respectively: We normalize scores from the autograder to the range 0-1 with min-max scaling, to use in our evaluation.

In order to verify that this autograder works properly, we perform a human evaluation using Amazon Mechanical Turk. We perform two human evaluations, one for the coherence score, and one for the steering performance score.

Coherence Score: We sample 100 examples from each coherence grade (from the computed rollouts from the steering experiment), for a total of 600 samples (100 controls, with no steering applied). We then compute a dataset of paired samples, using answers to the same question next to each other. We ask our mechanical turkers to select the most coherent response, getting 10 labels per prompt. Below is an example question asked to the graders.

[illegible]

Figure 10. **Example of Coherence Evaluation** A random sample from our dataset. Clearly, Answer 1 is more coherent.

Then, we compute the probability that the turker will prefer one answer to another, based on their respective grader scores.

Steering Score: To evaluate this, we first sample rollouts at each level of steering, as measured by our LLM grader. Then, we present the question-answer pairs to the human evaluators, asking them to select what concept aligns most

closely with the given response from a list of four classes (the target class for the steering vector, the original class of the image, and two distractors). An example of this task is given below.

Instructions

Shortcuts

Select the multiple choice option which most closely aligns with the completion.

Below you are provided with a question and text that answers the question (“Completion”). You are also provided four multiple choice keywords that could summarize the completion. Read the completion, and determine which of the four multiple choice keywords best matches the completion text.

Question: Is this image related in any way to the concept "shield"?

Completion: 1. The image shows a metal object with text on it, which appears to be a badge or a seal. The text is partially obscured, but it seems to include the word "shield." 2. The object itself could be interpreted as a shield, as it is a circular emblem with a border that might be designed to protect or represent something. 3. The concept of a shield is often associated with protection, defense, or security. In this context, the object

Select an option

| | |
|--------|---|
| switch | 1 |
| lion | 2 |
| laptop | 3 |
| shield | 4 |

Figure 11. **Example of Coherence Evaluation** A random sample from our dataset. Clearly, the completion is most aligned with the class “shield”

We then compute the probability that the user selects the target and original class, given a steering score for the prompt. Using this, we find that our LLM autograder aligns well with human data.

B. Examples of Steering at Various Strengths

In figure 12, we provide a handful of examples of steered model completions. The steering creates hallucinations of content related to the target class, while maintaining a coherent description of the hallucinated image. Furthermore, at the intermediate steering levels, the original context of the image is maintained: the model hallucinates two humans in lion costumes, instead of two lions, in the second example, which transforms into two people wearing backpacks.

C. Multimodality Evaluation Details

We evaluate our trained SAEs and neurons throughout the model, looking for interpretable and multimodal features and neurons alike. In order to do this, we first sample 25 SAE features and 50 Neurons from layers 8,12,16,20,24, for a total of 250 features. We compute activation deciles for each feature across the ShareGPT dataset, using text and image activations separately. For each feature/neuron, we present the user with the given activation deciles in a “feature browser.” Below is an example browser, showing the image activations of a “boots” SAE feature.

We ask the user to provide text and image interpretations of each feature independently or to respond that the features are uninterpretable. Then, we ask the user if their descriptions of the text and image activation patterns match, to determine feature multimodality.



The image shows a chicken with a predominantly brown plumage, possibly a breed such as a Rhode Island Red or a similar variety. The chicken has a white tail and a white patch on its wing, which is characteristic of some breeds. It appears to be standing on a ground covered with leaves, suggesting it might be in an outdoor enclosure or a natural environment.

The image shows a roasted chicken with its skin crisped and golden brown. The chicken is placed on a bed of what appears to be dried leaves or herbs, which is a common way to serve a roasted bird. The setting suggests it might be a home-cooked meal, and the chicken is likely seasoned with herbs and spices before roasting.

The image shows a pizza with a thick crust, topped with what appears to be a red sauce, possibly tomato sauce, and cheese. The pizza is sliced and ready to be served. The pizza is placed on a surface that looks like a wooden table or a similar type of furniture.



This image shows two lions. They appear to be in a zoo or wildlife park setting, as indicated by the artificial grass and the white background. The lions are facing each other, and one of them is displaying a behavior known as "stern face" or "flehen response," which is a way for lions to communicate with each other. This behavior can be a sign of dominance or aggression.

The image shows two individuals dressed in costumes that resemble lions. They are standing side by side, with one person appearing to be roaring or speaking, and the other looking attentively. The costumes are detailed, with the mane, fur, and facial features designed to mimic a lion's appearance. The setting appears to be a studio or a similar indoor environment, as indicated by the plain background and the absence of any natural elements.

This image shows two people standing next to each other, each with a backpack on their back. They appear to be in a room with a white wall in the background. The person on the left is wearing a brown backpack, while the person on the right is wearing a black backpack. Both individuals are facing the same direction, and it seems like they are either preparing to leave or have just arrived at their destination.



The image shows a black pot sitting on a stove top. The stove has a control panel with knobs, and there's a reflection of the pot in the surface of the stove. The lighting in the photo gives it a warm, orange hue. The pot appears to be made of cast iron, which is a common material for pots and pans due to its durability.

The image shows a close-up of a person's hands holding a pot on a stove. The stove has a control panel with two knobs, and there's a reflection of the person in the pot's handle. The background is blurred, but it appears to be a kitchen setting with a patterned wall and a mirror. The focus is on the pot and the stove, with the person's hands and the stove's control panel being the main subjects of the photo.

The image shows a man dressed in formal attire, standing at a podium with a microphone, suggesting he is about to give a speech or presentation. He is wearing a suit with a tie, and there is a tie visible in the foreground. The setting appears to be indoors, possibly at a formal event or ceremony. The man is looking directly at the camera, and there is another person in the background who is also dressed formally, wearing a suit and tie.



The image shows a person posing on a basketball court. The individual is wearing a basketball uniform with the number 31 and the word "CLEVELAND" on the front, suggesting they are a member of a basketball team from Cleveland. They are holding a basketball and smiling at the camera. The background features basketball hoops and a scoreboard, indicating that this is a basketball court.

The image shows a person holding a yellow object, which appears to be a fruit or a vegetable, possibly a lemon or a grapefruit. The person is wearing a bright yellow top, which matches the color of the object they are holding. The background is a simple, solid color, which helps to focus attention on the person and the object. The lighting in the photo is bright and even, suggesting it might have been taken in a well-lit indoor space.

The image shows a person wearing a bright yellow top. The person is standing against a light background, and the lighting appears to be natural, possibly from sunlight. The image is a close-up, focusing on the upper body and the top of the person's head. The bright yellow color of the top stands out prominently.

Figure 12. **Steering Examples** Several selected examples of image-token steering. Three image descriptions are taken, with the simple prompt: "What is this image?", at three steering levels. The first sample is steered towards "pizza", the second is steered towards "backpack", the third is steered towards "groom", and the fourth is steered towards "lemon".

Max Image Exemplars (Average Activation <0.126)



Max Image Exemplars (Activation $0.126 - 0.084$)



Max Image Exemplars (Activation $0.084 - 0.042$)

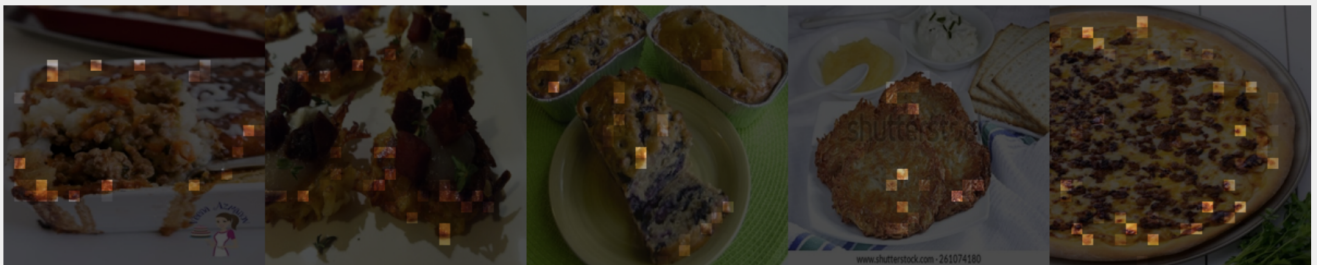
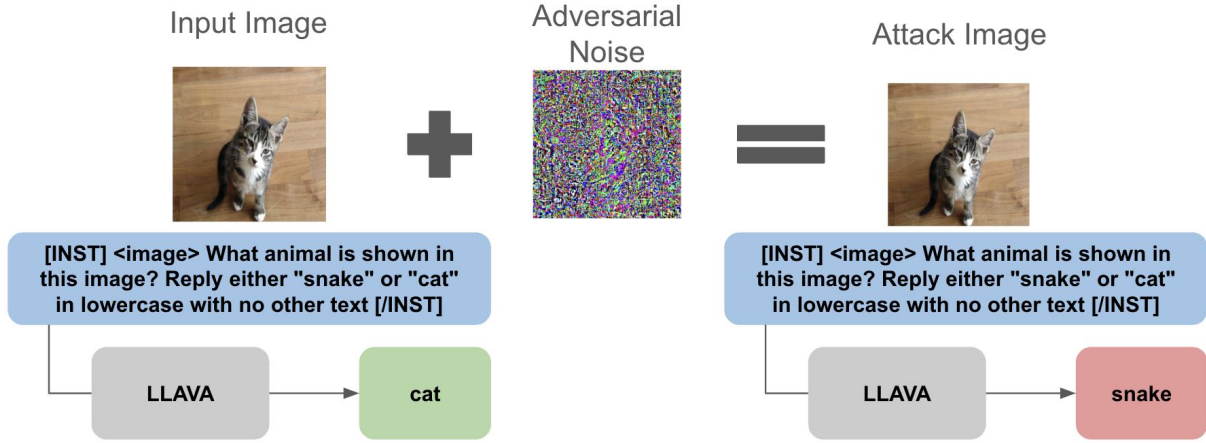


Figure 13. **Example of a browser:** This SAE feature appears to activate on images of crust and baked goods.

D. Adversarial Attacks on VLLMs



Although we find that the image understanding of the model is highly steerable through linear representations, we wonder how other interventions are expressed in the model representations. To do this, we study the setting of Adversarial Attacks, using gradient descent to optimize perturbations to edit the model response. Specifically, we use a single prompt, and optimize the difference in log-probs between an initial and target class using PGD, as shown in section D.

We ask, how does the Adversarial Attack change model internals? Although we hoped to find that the adversarial attack was well-explained by the SAE basis, we found that the difference in activation between the original and adversarially attacked images were usually **dense**, involving hundreds of SAE features. Furthermore, the SAE features which changed the most between the images appeared to be random, with them not directly corresponding to the change of the adversarial attack.

Furthermore, we found that adversarial attacks were quite “brittle”, with noise which succeeded in editing model output on one prompt not generalizing well to other prompts. This made experimentation quite tricky. We thus urge further work to consider this setting.